Strengthening Characteristics of Nitrogen-Alloyed 201 Stainless Steel

J. Rawers and G. Slavens

Strengthening characteristics of 201 stainless steel under nitrogen enhancement from zero to approximately 1.5 wt % N concentration are improved with increasing nitrogen. Yield and tensile strength, strain hardening, and cold-work/hardness relationships are proportional to nitrogen concentration. Strengths increased with increasing nitrogen up 1.0 wt %, even though at nitrogen concentrations greater than 0.65 wt %, Cr_2N precipitates formed. Strengthening models from tensile and cold working are discussed, compared, and correlated to nitrogen concentration, tensile properties, and microstructure.

Keywords
mechanical properties, nitrogen steels, type 201 stainless steel

1. Introduction

THIS STUDY has been designed to characterize the effects of nitrogen addition on the strength properties of commercial stainless steel. A common perception is that increasing nitrogen concentration is accompanied by formation of precipitates, resulting in a decrease in tensile properties. This study shows that, under certain processing conditions, precipitate formation may increase tensile properties. True stress/true strain properties are shown to be readily related to the change in hardness with increasing cold working.

Selected characteristics of stainless steels have been shown to be a function of interstitial nitrogen concentration (Ref 1-13). In turn, the nitrogen concentration is a function of alloy composition and melt environment. Chromium and manganese increase nitrogen solubility, whereas nickel decreases nitrogen solubility (Ref 7, 8). Several commercial stainless steels have alloy compositions specially designed to take advantage of the enhanced properties that can be obtained with higher nitrogen-concentration levels. These properties include improved tensile strength, wear, corrosion protection, and fatigue resistance (Ref 14).

For most face-centered cubic (fcc) iron alloys the maximum interstitial nitrogen concentration required for optimal tensile strength is not obtained by melting at atmospheric pressure. Melting under elevated nitrogen pressures has been used to increase nitrogen concentration (Ref 15-17). Several studies have shown that the nitrogen concentration in liquid iron follows Seivert's law; that is, it is proportional to the square root of the nitrogen melt pressure (Ref 18). Because the nitrogen solubility of fcc-Fe alloys is greater in the solid phase than it is in the liquid phase (Ref 19), the nitrogen concentration obtained in the liquid phase is retained during solidification.

Strengthening characteristics of nitrogen-enhanced steels have been the subject of three international conferences (Ref 1-3). To date, however, few experimental attempts have been made to correlate different strengthening mechanisms (e.g., tensile and cold-work characteristics) for a single alloy composition from low nitrogen concentrations through nitrogen saturation. In the present study, correlations between tensile and cold-work characteristics and nitrogen concentration were determined for a commercial-grade 201 stainless steel composition. A model for the role of nitrogen in strengthening is proposed.

Interstitial nitrogen increases both the yield strength and the tensile strength of fcc-Fe alloys (Ref 9, 10, 12, 13, 20, 21). The influence of nitrogen on yield strength has been shown to be a function of temperature. Below room temperature, nitrogen strengthening is proportional to the square root of the nitrogen interstitial concentration. At higher temperatures, nitrogen strengthening changes and becomes linearly proportional to the nitrogen concentration.

Strain-hardening studies have shown that for many fcc-phase materials, especially stainless steels (Ref 22-25), the Ludwik (Ref 6) (or Hollomon, Ref 27) relationship ($\sigma = K\varepsilon^n$, where σ is true stress, ε is true strain, and K and n are empirical constants) is not valid over the full range of the true stress/true strain curve. At higher stress or strain levels, the Ludwik equation is valid; however, at lower strain values, positive deviations from the Ludwik equation are observed. Several empirical and theoretical attempts have been made to modify the Ludwik equation (Ref 3) to accommodate this observed deviation. Studies have shown that nitrogen-enhanced 300 series stainless steels modify strain-hardening equations (Ref 24, 25, 28).

2. Experimentation

The nitrogen concentration in a commercial-grade 201 stainless steel (201SS) was increased from 0.060 wt% to greater than 1.45 wt% by high-pressure melting (Ref 29). The base material was obtained from Allegheny Ludlum Steel heat no. 851296. Alloy composition is presented in Table 1. Samples weighing approximately 2.5 kg were melted under nitrogen pressures from 0.01 to 6.5 MPa. After 30 min of induction melting, the samples were withdrawn from the induction zone, resulting in an ingot without a shrinkage hole and with uniform nitrogen concentration throughout.

The ingots were hot rolled into sheet, annealed, and then cut into strips for tensile testing and cold working. Tensile tests were performed at room temperature following ASTM E8. The gage section of the tensile samples was 50 mm by approximately 6.1 by 3.2 mm. Tensile tests were conducted in two stages. During the first stage, strain of the gage length was monitored by a strain-gage extensometer up to approximately 3

J. Rawers and **G. Slavens,** Albany Research Center, U.S. Bureau of Mines, Albany, OR, USA 97321-2198.

to 5% total strain. The test was then interrupted, the strain gage removed, and the tensile test continued up to rupture. The tensile head displacement was monitored and used to determine sample tensile elongation.

In addition to evaluation of tensile characteristics, strips of each alloy composition were reduced by a series of cold-rolling steps. After each cold-roll step, hardness measurements were taken.

Nitrogen concentrations were determined from segments cut from the fabricated sheets and fractured tensile samples, both by Kjeldahl analysis and with a LECO TC436 gas analyzer (LECO Corp., Bellefonte, PA). Phase identification and microstructure of the ingots and rolled sheet were obtained using x-ray diffraction (XRD), scanning electron microscopy (SEM), and transmission electron microscopy (TEM). Phase composition and concentration were determined by XRD of polished sections of the annealed sheets. Microstructure was determined by optical and SEM analysis of cross-sectional samples of the annealed sheets.

To evaluate the subgrain microstructure of the samples that had undergone plastic deformation, TEM samples were cut from the gage section of tensile bars that had been pulled to failure. Samples were from a region of local deformation near the fracture surface. The tensile axis was approximately parallel to the surface of the samples in all cases. Samples were ground and electropolished to electron transparency using conventional techniques, with an electrolyte of 90 vol% acetic acid and 10 vol% perchloric acid. Transmission electron analyses were performed at 100 kV on a Hitachi H-600 microscope (Hitachi Electronics, Kyoto, Japan).

Table 1 Alloy composition of base metal (weight percent)

Chromium	16.2
Nickel	4.89
Manganese	7.11
Nitrogen	0.06
Carbon	0.07
Phosphorus	0.04
Sulfur	0.001
Silicon	0.49
Iron	bal

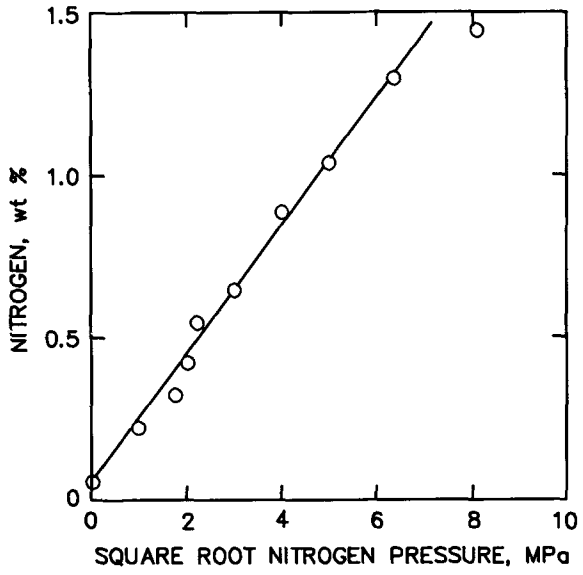

Fig. 1 Nitrogen concentration as a function of the square root of the nitrogen melt pressure used during melting

3. Data and Analysis

After melting, the samples were analyzed for nitrogen concentration. They were then sectioned and their microstructure determined using microscopy and XRD. Nitrogen distribution could then be determined by comparing the measured lattice expansion against previously determined relationships for lattice expansion with increasing interstitial nitrogen concentration. After hot-roll fabrication, tensile samples were cut from the sheet. Tensile properties were related to the sample nitrogen concentration and microstructure. Samples were also cold worked, and the cold-work properties were again related to the nitrogen concentration and microstructure. Correlations between the tensile and cold-work properties were assessed.

Nitrogen analysis showed that for melting under nitrogen melt pressure up to 4.0 MPa, the nitrogen concentration in the castings was proportional to the square root of the nitrogen melt pressure during melting (Fig. 1), even though at elevated pressures the casting contained chromium nitride precipitates:

$$(\text{N, wt\%}) = 0.59\ (\text{pressure, MPa})^{0.5} \qquad \text{(Eq 1)}$$

At higher pressures, a slight negative deviation from the linear relationship began to develop. Similar results have been reported in previous high-pressure experiments (Ref 4, 5).

Nitrogen concentration reached 1.45 wt% when melted under 6.5 MPa. X-ray diffraction analysis determined that for all samples, except the as-received material, the matrix was fcc-Fe. The as-received material contained approximately 2 wt% bcc-Fe.

The nitrogen concentration remained interstitial until the total nitrogen concentration exceeded 0.65 wt%. Backscattered SEM examination of the microstructure showed that with increasing nitrogen concentration, the as-cast dendritic structure of the ingot became apparent (Fig. 2). With increasing nitrogen concentration, fine Cr_2N precipitates developed in the outer dendritic regions (Fig. 2b); however, the inner regions of the dendritic structure remained precipitate free. The Cr_2N precipitates were distributed throughout the grain microstructure, not concentrated on the recrystallized grain boundaries. With further increase in nitrogen concentration, the Cr_2N precipitate distribution extended farther into the center portion of the dendrite (Fig. 2c). Eventually the entire sample was saturated with Cr_2N precipitates (Fig. 2d).

Examination by TEM of the grain cell structure from the plastically deformed region showed a similar dislocation structure for all nitrogen concentrations, even in the presence of Cr_2N precipitates. Although no direct measurement of the amount of plastic deformation for the TEM samples was possible, if one assumes that there was uniform deformation throughout the gage region until localized plastic deformation occurred, then the observed grain microstructure in this region was that of plastic deformation at the tensile strength, that is,

just before local necking occurred (Fig. 3). The plastic deformation varied from a minimum of 15% for samples with Cr_2N precipitates to greater than 80% for the as-received sample.

No sample showed signs of dislocation cell wall development. The bcc-Fe detected by XRD of the as-received sample appeared as separate grains, indicating that the bcc-Fe grains formed during melt-solidification and not as a result of solid-state phase change or plastic deformation (Fig. 3). Martensite was observed in the grain boundaries of samples with less than 0.35 wt% N. In all samples, extensive twinning was observed.

The lattice microstructure expands with increasing interstitial nitrogen concentration (Ref 8, 15). Results from this study showed a linear change in lattice *d*-spacing (as measured by XRD) with increasing nitrogen concentration (as determined by LECO analysis) until the nitrogen concentration exceeded 0.65 wt% (Fig. 4).

$$[(110)\text{-Fe } d\text{-spacing, nm}] = 0.2027[\text{nm}] + 0.0018\ [\text{N, wt\%}] \quad \text{(Eq 2)}$$

The rate of increase, 0.0018 nm/[N, wt%], was similar to the previously reported value of 0.002 nm/[N, wt%].

The interstitial nitrogen solubility limit in 201SS was determined by XRD to be between 0.55 and 0.65 wt%, approximately twice the nitrogen concentration level reached in commercial-grade 201SS by conventional melting practices. With the formation of Cr_2N precipitates, the fcc-Fe lattice *d*-spacing decreased (Table 2). The Cr_2N concentration was determined from the relative intensity of the XRD peaks. Statistical analysis showed a linear increase in the Cr_2N concentration with increasing nitrogen concentration (Fig. 5).

$$[Cr_2N, \text{wt\%}] = 3.7\ ([\text{N, wt\%}] - 0.53) \quad \text{(Eq 3)}$$

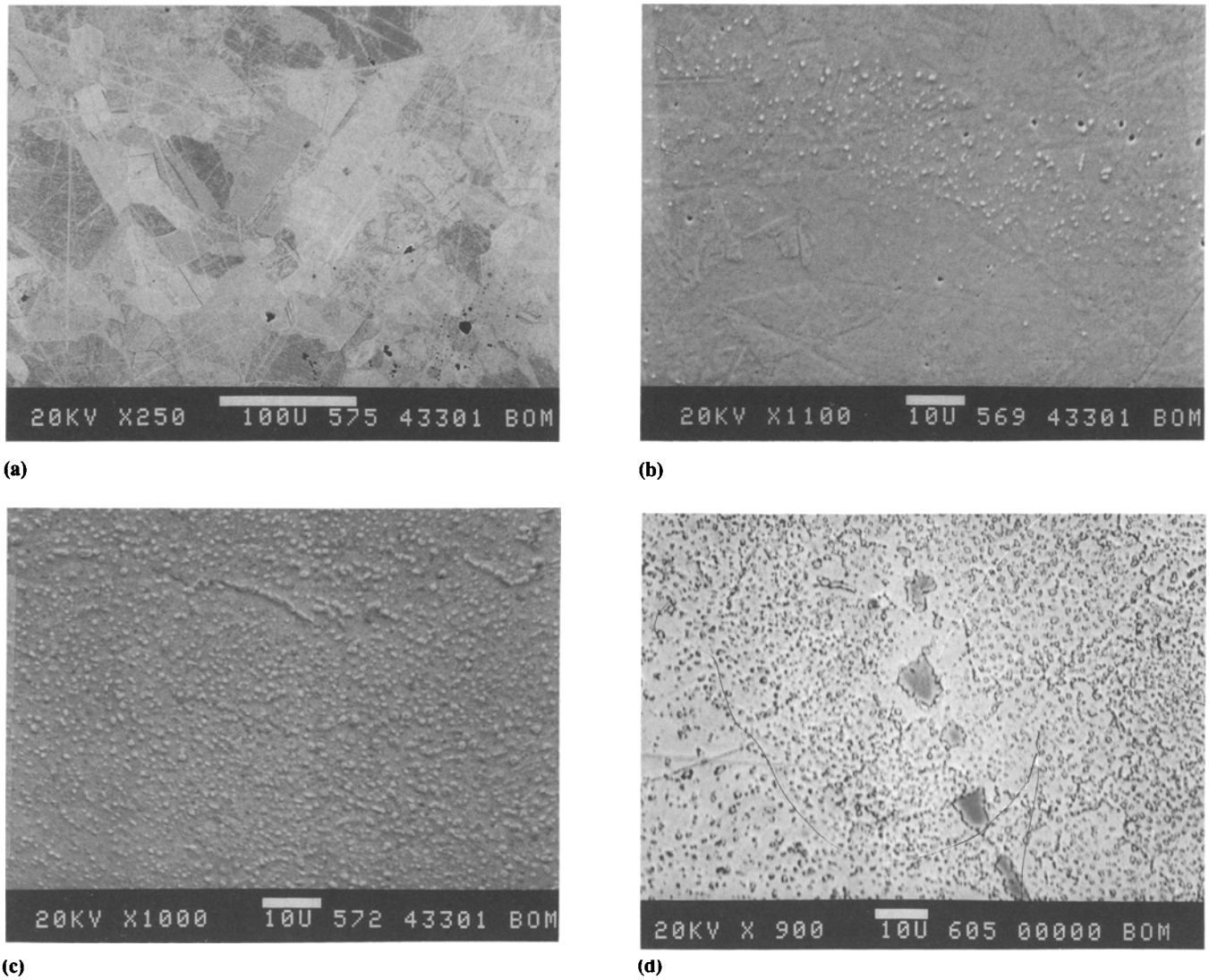

(a) (b) (c) (d)

Fig. 2 Scanning electron micrographs of 201SS after melting as a function of nitrogen concentration. (a) As received. (b) With 0.65 wt% N. Note the formation of Cr_2N precipitates in the region of as-cast dendritic arms. (c) With 0.88 wt% N. Note increasing Cr_2N precipitates throughout the matrix. (d) With 1.21 wt% N. Note the Cr_2N precipitates throughout the entire matrix and along grain boundaries.

Yield and tensile strengths were analyzed as a power function of nitrogen concentration:

$$(\sigma_{YS\&TS}, \text{MPa}) = (\sigma_0, \text{MPa}) + k[\text{N, wt\%}]^n \quad \text{(Eq 4)}$$

The increase in yield and tensile strengths with increasing nitrogen concentration was observed to continue up to approximately 1.0 wt% N (Table 1). (Table 2 also contains data from a previous nitrogen 201SS experiment [Ref 5, 6]). This increase in tensile strength continued with increasing nitrogen concentration even though above 0.55 wt% N the increase in concentration results in the formation of Cr_2N precipitates, which decreased the interstitial nitrogen and chromium concentration in the matrix.

Plots of yield strength as a function of the nitrogen concentration (athermal) (Fig. 6a) or of the square root of the nitrogen concentration (thermal) (Fig. 6b) suggest that, at room temperature, nitrogen strengthening in 201SS is predominantly described by the square root of the nitrogen concentration. Thus, the nitrogen-strengthening mechanism at room temperature is predominantly thermal, with a small athermal component. The statistical model that most closely fitted the data had a nitrogen exponent slightly above 0.5, indicating that at room temperature the nitrogen-strengthening transition from thermal to athermal was just beginning (Table 3).

The yield strength at maximum nitrogen solubility, approximately 0.6 wt%, was 510 MPa, a 50% increase over the nominal yield strength of annealed commercial-grade 201SS (Ref 14). Thus, for a modest increase in melt pressure, <0.5 MPa, a significant increase in yield strength resulted. The maximum yield stress, 752 MPa, was obtained with a nitrogen concentration of approximately 1.0 wt%, which was three times the yield strength for the as-received stainless steel.

Tensile strength was also a function of nitrogen concentration and the presence, or absence, of Cr_2N precipitates. Tensile strength increased with increasing nitrogen concentration until approximately 1.0 wt% (Fig. 7a and b). As with yield strength, the increase

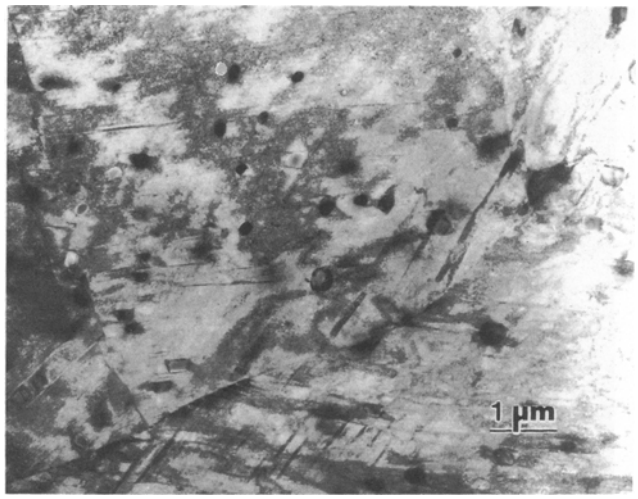

(a)

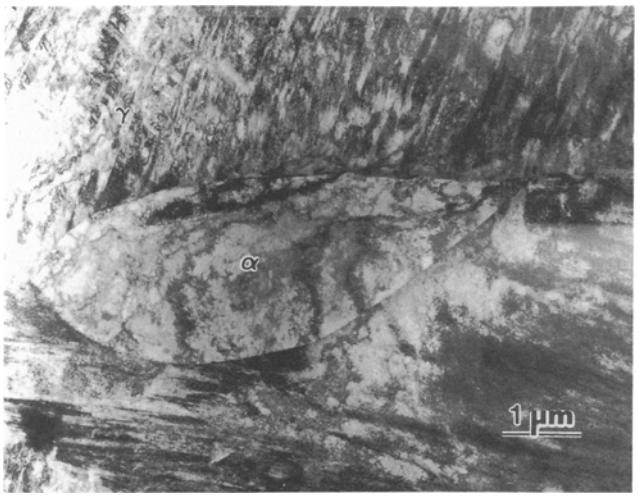

(b)

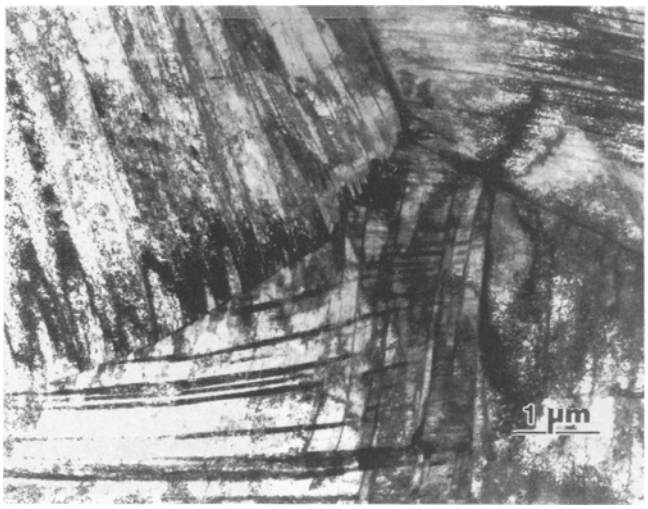

(c)

Fig. 3 Transmission electron micrographs of 201SS. (a) With 0.65 wt% N. Note the appearance of Cr_2N precipitate clusters. (b) With 0.06 wt% N. Note the appearance of α-Fe phase between grains of γ-Fe. (c) With 0.35 wt% N. Martensite is observed to be present at the grain boundaries.

in tensile strength continued even though above 0.65 wt% Cr_2N precipitates began to form. Previous studies have provided explanations for the nitrogen-strengthening effects to be either linear or quadratic (Ref 17). Statistical analysis suggests that the correlation between tensile strength and nitrogen concentration is somewhere between linear and quadratic (Table 3).

Several different analyses of the stress-strain curves (Fig. 8) were used to characterize strain hardening as a function of increased nitrogen concentration. Plots of $\ln(\sigma)$ versus $\ln(\varepsilon)$ (Fig. 9) show that while at higher strains a definite linear region existed, at lower strains there were positive deviations from linearity. The strain at the point of departure from linear is shown in Fig. 10. This point, defined as the "breaking point" in Table 4, rapidly decreased with increasing nitrogen concentration. A plot of the yield, breaking, and tensile strengths as a function of nitrogen concentration (Fig. 11) shows that there was a strong correlation between the breaking and tensile strengths.

As pointed out in section 1, strain hardening of fcc materials, especially stainless steels, cannot be described over the entire true stress/true strain curve by the Ludwik equation:

$$(\sigma, \text{MPa}) = K\varepsilon^n \qquad \text{(Eq 5)}$$

where K is a strength factor (theoretical true stress at a true strain of 1.0) and n is a strain-hardening exponent.

Table 2 Chemistry, tensile, microstructure, and XRD analysis

[N]LECO, wt%	[N]KJ, wt%	Magnetic property	Cr_2N, %	Yield stress, MPa		Tensile stress, MPa		Elongation, %		X-ray, nm (110)-Fe	Microscopy
0.06		Very magnetic	0.0	254	273	741	774	110	115	0.2077	SEM/TEM
0.23	0.24	Slightly magnetic	0.0	427	423	765	782	82	94	0.2080	SEM/TEM
0.33	0.33	Nonmagnetic	0.0	464	466	807	808	91	86	0.2081	
0.43	0.44	Nonmagnetic	0.0	474	498	847	895	77	84	0.2083	SEM/TEM
0.55	0.51		0.0	503	524	899	894	74	77	0.2083	
0.65	0.64		0.31	570	585	961	976	68	74	0.2085	SEM/TEM
0.89	0.88		1.54	677	720	1138	1134	58	47	0.2086	
1.04	1.03		1.94	752	760	1165	1175	43	48	0.2085	
1.30	1.10		2.64	734	712	1144	1132	25	22	0.2084	SEM/TEM
1.45	1.21		3.49	750	734	1090	1139	14	20	0.2084,	

Tensile results from previous high-nitrogen tensile tests of 201SS(a)

[N]LECO, wt%	[N]KJ, wt%	Magnetic property	Cr_2N, %	Yield stress, MPa		Tensile stress, MPa		Strain hardening(b)
0.071	0.080	...	0.0	261	...	507	...	0.28
0.57	0.57	...	0.0	549	...	897	...	0.18
1.24	1.18	...	2.24	741	...	1155	...	0.14

(a) Source: Ref 5 and 6. (b) See Table 6.

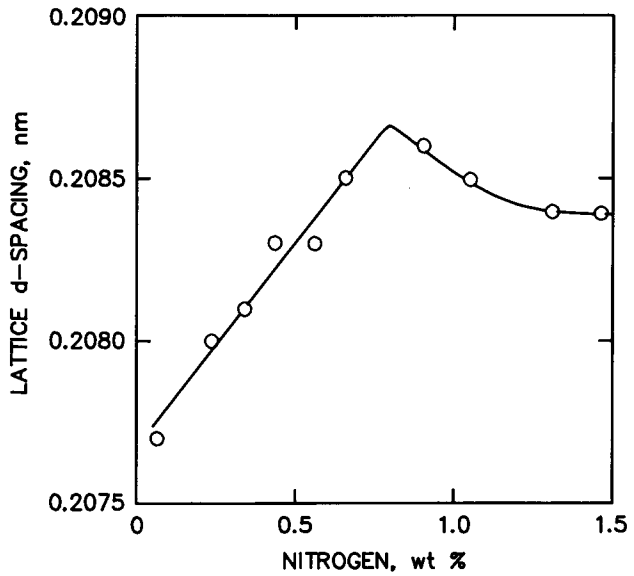

Fig. 4 Lattice *d*-spacing of the (110)-Fe plane as a function of nitrogen concentration

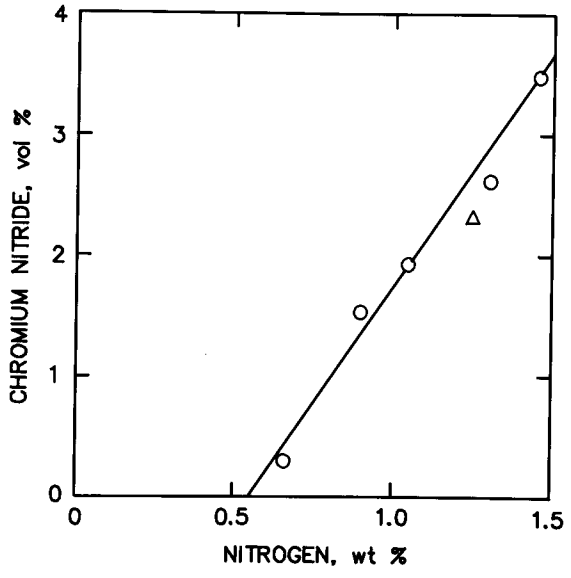

Fig. 5 Chromium nitride concentration as a function of total nitrogen concentration

Several different approaches to evaluation of the full true stress/true strain curves are presented in Table 4. The first expression studied was the simple Ludwik equation:

$$\sigma = K\varepsilon^n \quad \text{(Eq 5a)}$$

The next expression examined was for the Ludwik equation applied only to stress values above the "breaking point":

$$\sigma = K'\varepsilon^{n'} \quad \text{(Eq 5b)}$$

The third expression was a slight simplification of Ludwigson equation (Ref 24):

$$\sigma = K\varepsilon^n + \Delta,\ \Delta = [k_1 \exp(m\varepsilon)]$$

where Δ was set equal to σ_{YS}:

$$\sigma = K\varepsilon^n + \Delta,\ \Delta = \sigma_{YS} \quad \text{(Eq 5c)}$$

The only sample with sufficient data for which the full Ludwigson expression (i.e., $\Delta = [k_1 \exp(m\varepsilon)]$) could be used was the as-received material. Data for the full Ludwigson expression and several other stainless steels and nitrogen-enhanced stainless steels are presented in Table 5. The fourth expression, proposed by Swift (Ref 30), was:

$$\sigma = K(\varepsilon_0 + \varepsilon)^n \quad \text{(Eq 5d)}$$

Statistical analysis was conducted using nonlinear regression analysis. Since all the strain-hardening exponents showed similar trends, only the second expression—the Ludwik equa-

Table 3 Statistical fit of tensile data

Square root			Linear			Quadratic			Nonlinear			
σ_0	K	R^2	σ_0	K′	R^2	σ_0	K″	R^2	σ_0	K*	n	R^2
$\sigma_{YS} = \sigma_0 + K[N, wt\%]^{0.5}$			$\sigma_{YS} = \sigma_0 + K'[N, wt\%]$			$\sigma_{YS} = \sigma_0 + K''[N, wt\%]^2$			$\sigma_{YS} = \sigma_0 + K^*[N, wt\%]^n$			
107	608	0.98	281	450	0.95	385	341	0.91	210	520	0.72	0.99+
$\sigma_{BK} = \sigma_0 + K[N, wt\%]^{0.5}$			$\sigma_{BK} = \sigma_0 + K'[N, wt\%]$			$\sigma_{BK} = \sigma_0 + K''[N, wt\%]^2$			$\sigma_{BK} = \sigma_0 + K^*[N, wt\%]^n$			
354	629	0.92	516	509	0.97	671	447	0.99	599	460	1.72	0.99+
$\sigma_{TS} = \sigma_0 + K[N, wt\%]^{0.5}$			$\sigma_{TS} = \sigma_0 + K'[N, wt\%]$			$\sigma_{TS} = \sigma_0 + K''[N, wt\%]^2$			$\sigma_{TS} = \sigma_0 + K^*[N, wt\%]^n$			
524	582	0.93	677	468	0.97	773	405	0.98	737	430	1.49	0.99+

Table 4 Tensile true stress/true strain analysis

				Ludwik		Modified Ludwik		Ludwigson			Swift		
Melt pressure,	$[N]_{LECO}$,	"Breaking"		$\sigma = K\varepsilon^n$		$\sigma = K'\varepsilon^{n'0} > K_{BR}$		$\sigma = K\varepsilon^n + \Delta, \Delta = \sigma_{YS}$			$\sigma = K(\varepsilon_0 + \varepsilon)^n$		
MPa	wt%	σ_{BK}	ε_{BK}	K	n	K′	n′	K	n	Δ	K	n	ε_0
...	0.06	610	0.070	1570	0.34	2176	0.49	2380	0.73	265	2573	0.69	0.056
0.1	0.23	635	0.032	1244	0.19	1376	0.23	1286	0.53	425	1483	0.29	0.019
0.3	0.33	665	0.026	1308	0.18	1383	0.21	1301	0.52	465	1450	0.24	0.011
0.4	0.43	699	0.026	1354	0.18	1452	0.20	1306	0.49	486	1526	0.24	0.014
0.5	0.55	757	0.026	1425	0.17	1551	0.21	1391	0.49	514	1636	0.25	0.017
0.9	0.65	812	0.026	1600	0.16	1815	0.23	2050	0.48	578	2026	0.30	0.020
1.6	0.89	1012	0.026	1795	0.15	1966	0.18	1803	0.47	720	2260	0.25	0.017
2.5	1.04	1070	0.022	1728	0.13	1828	0.14	1555	0.43	760	1904	0.16	0.005
4.0	1.30	963	0.007	1654	0.11	1668	0.11	1274	0.33	712	1593	0.10	≈0
6.5	1.45	963	0.007	1659	0.11	1659	0.11	1310	0.35	734	1602	0.10	≈0

Table 5 Ludwigson expression for nitrogen-enhanced and several other stainless steels

Alloy designation	Nitrogen, wt%	k, MPa	n	k_1, MPa	m	Ref
316	0.029	1161	0.35	4.95	–57	25
	0.080	1182	0.36	5.09	–79	
	0.120	1302	0.35	5.26	–68	
	0.250	1513	0.35	5.42	–65	
304	...	1921	0.48	7.33	–24	24
	...	1578	0.44	7.05	–25	(average of 10 steels)
17Cr-15Mn	0.4	1340	0.51	6.89	–17	24
19Cr-5Ni-5Mn	0.70	2106	0.47	6.02	–24	28
As received	0.06	2385	0.54	5.46	–24	...

tion for stress-strain data taken past the breaking point—will be discussed in detail.

The strain-hardening coefficient, n, for the as-received material with low nitrogen concentration was approximately that of fcc-phase materials: ≈0.30 to 0.50. With increasing nitrogen concentrations from 0.23 to 0.65 wt% N, the strain-hardening exponent rapidly decreased to a nearly constant value, ≈0.10 to 0.20, consistent with bcc-phase steels. When Cr_2N precipitates developed above 0.65 wt% N, the exponent again began to rapidly decrease (Table 4, Fig. 12, Ref 28).

The strength factor (K, Eq 5) was proportional to the nitrogen concentration (Table 4). Except for the sudden drop in value between the as-received material (0.06 wt% N) and the first nitrogen melt ingot (0.23 wt% N), the strength factor increased with increasing nitrogen concentration until shortly after the formation of Cr_2N precipitates (Fig. 13). For the strength factor in the Ludwik equations (Eq 5a and b), the exponent, n, has a value of 1.5. Statistical analysis showed the strength factor to have a nitrogen dependence similar to that of the tensile strength (Eq 4):

$$(K, MPa) = a + b[N, wt\%]^n \quad \text{(Eq 6)}$$

Because of the influence of two strain-hardening mechanisms, one during the initial stage of straining and the second after sig-

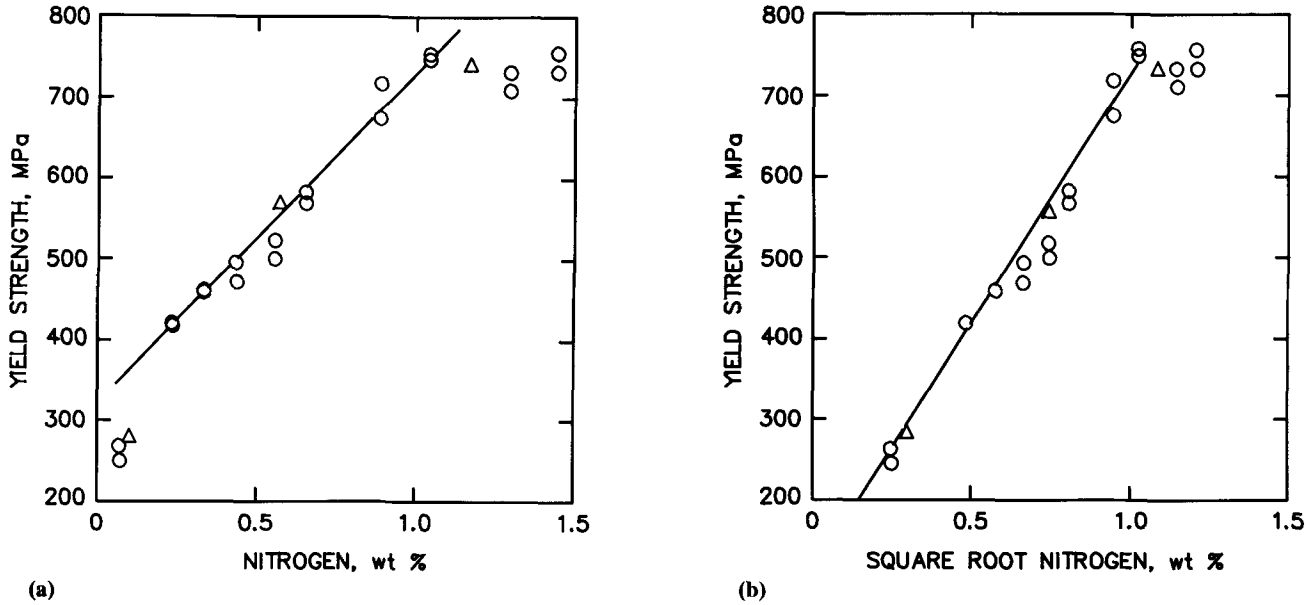

Fig. 6 (a) Yield strength as a linear function of nitrogen concentration. (b) Yield strength as a square root function of nitrogen concentration

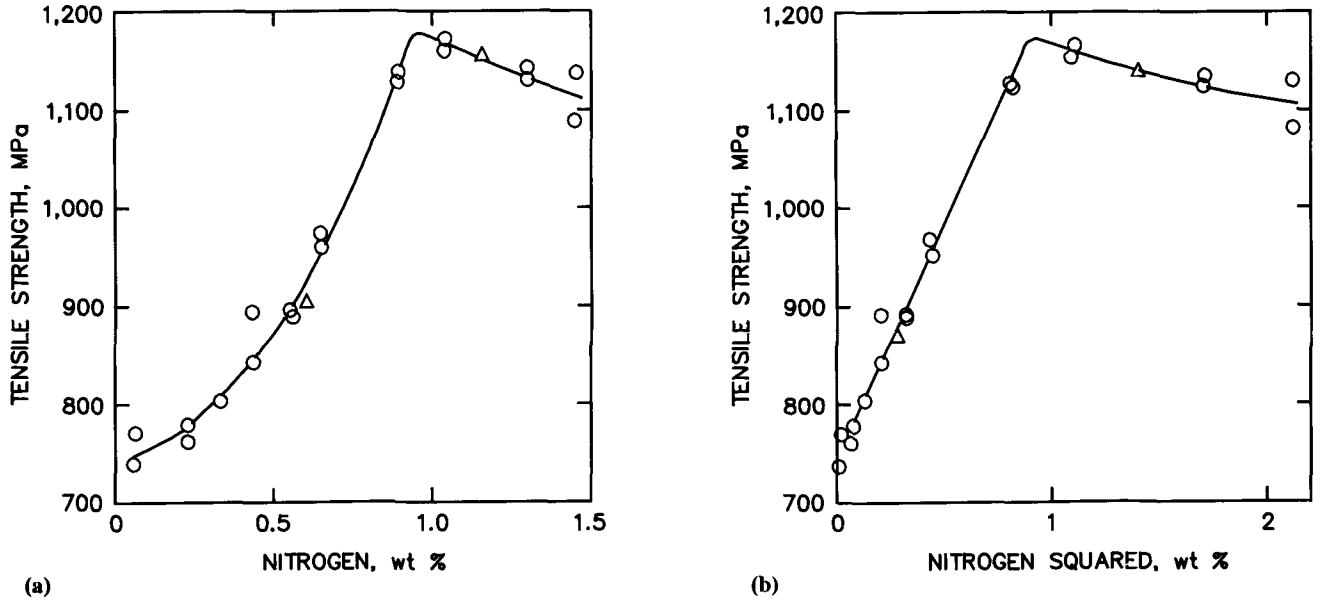

Fig. 7 (a) Tensile strength as a linear function of nitrogen concentration. (b) Tensile strength as a function of nitrogen concentration squared

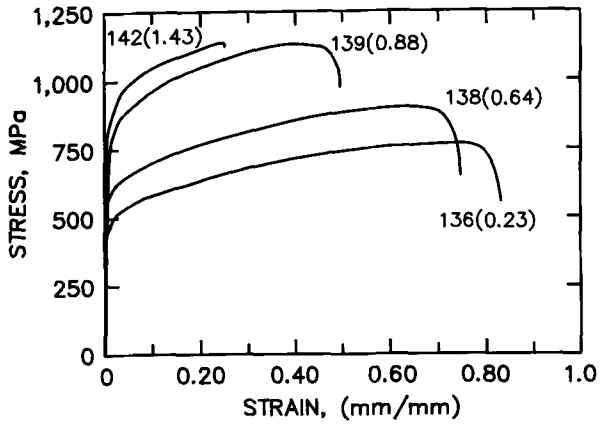

Fig. 8 Stress-strain curves for several 201SS steels with differing nitrogen concentrations: 0.23 wt% (run no. 136), 0.64 wt% (run no. 138), 0.88 wt% (run no. 139), and 1.43 wt% (run no. 142)

nificant deformation, it was not possible to develop a single expression relating stress/strain/nitrogen. Strain-hardening analysis suggested that for strains after the breaking point (or breaking stress) a simple linear expression (Eq 5b) was appropriate. Tensile correlations were also found to be a simple expression of nitrogen concentration (Eq 4). A simple expression relating strain-hardening and nitrogen dependence for the second stage of strain hardening was derived by combining Eq 4, Eq 5, and an interaction term between nitrogen and strain:

$$\sigma = \alpha\varepsilon^{\beta} + \gamma[N]^{\delta} + \zeta\varepsilon^{\beta}[N]^{\delta} \quad \text{(Eq 7)}$$

where α = 1323 MPa; ε = true strain; β = 0.26; γ = 568 MPa; [N] = nitrogen concentration, wt%; δ = 1.37; ζ = interaction term, −13.3; and R^2 = statistical fit, 0.997.

Exponents and coefficients for Eq 7 are similar to those previously determined (Tables 3 and 4). The strain-hardening coefficients and exponents are similar to the modified Ludwik expression. The nitrogen dependence coefficient, 568 MPa, is similar to the "breaking point" stress value, 509 MPa (Table 3), and the strain-hardening exponent term, 0.26, is similar to that determined for the tensile stress expression, 0.1 (Table 4).

Cold working is a common technique employed to strengthen metals. Metals respond similarly to cold working and to tensile strain hardening. Therefore, a similar relationship between nitrogen addition and strain hardening is to be expected. The hardness of a material is related to its resistance to plastic deformation and as such is an indication of the matrix strengthening, dislocation generation, dislocation motion, and the amount of plastic deformation already present in the material. Thus, for a given nitrogen concentration, the hardness/cold-work relationship should be similar to previously described tensile characteristics. During cold working the metal becomes strain hardened (Table 6, Fig. 14). This relationship can be expressed by:

$$\text{Hardness} = a + k(\%\ \text{cold work})^{n} \quad \text{(Eq 8)}$$

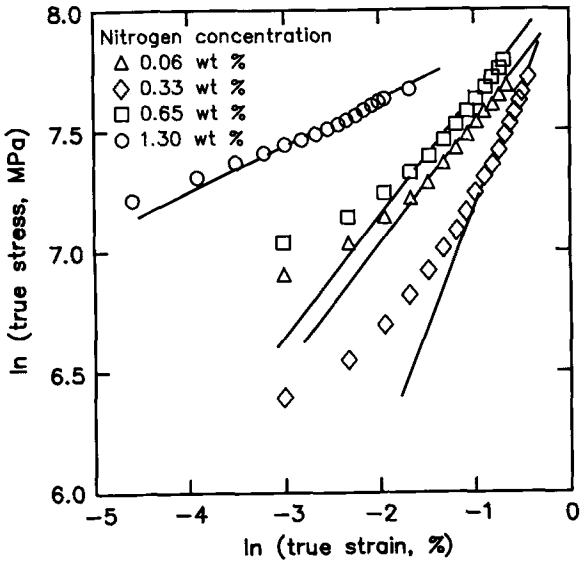

Fig. 9 True stress/true strain tensile curves for the tensile curves shown in Fig. 8

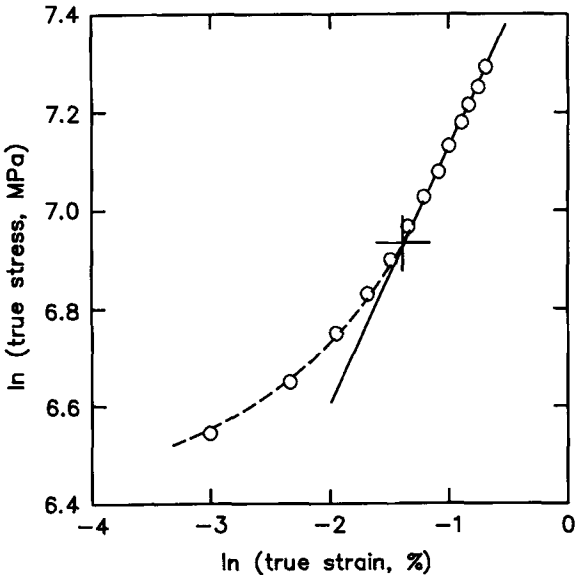

Fig. 10 True stress/true strain curve showing the nonlinear low-strain region and the higher-strain linear region. The point of departure (+) from nonlinear to linear is defined as the breaking point.

Values for the constants and exponents for several different nitrogen concentrations are presented in Table 7. The values of the constant, k, and the exponent, n, were approximately constant for interstitial nitrogen concentrations.

Hardness was also a function of matrix strength, which is related to alloy composition (i.e., nitrogen concentration (Fig. 15):

$$\text{Hardness} = \alpha + \beta\,[N, \text{wt\%}]^{\gamma} \quad \text{(Eq 9)}$$

Values for the coefficients α, β, and γ for several different cold-working conditions are presented in Table 7. Except for the as-

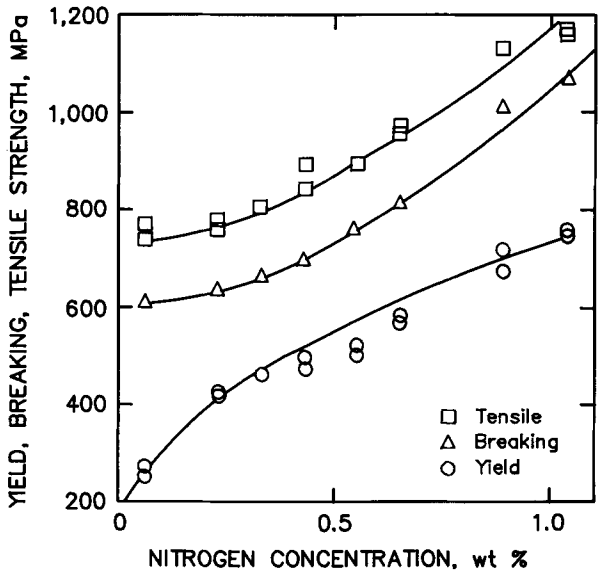

Fig. 11 Yield, breaking, and tensile strengths as a function of nitrogen concentration

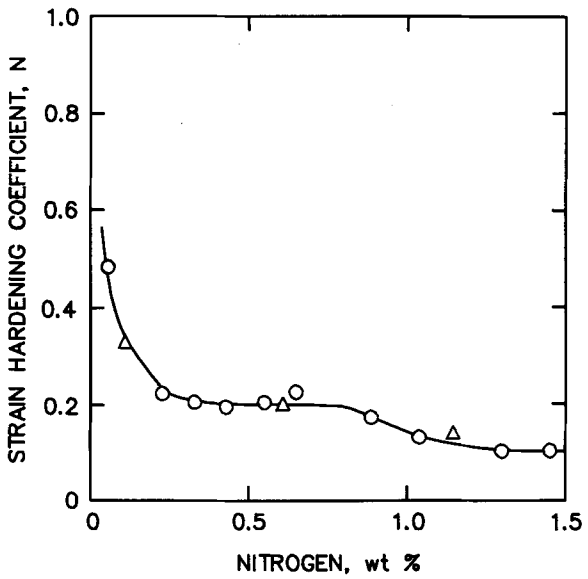

Fig. 12 Strain-hardening coefficient, n, as a function of nitrogen concentration

Table 6 Hardness measurements (HRA) of cold-worked samples as a function of nitrogen composition

$[N]_{LECO}$,	Cold rolling, %								
wt%	0	2	5	10	15	20	30	50	75
0.06	52.4	55.1	58.7	63.7	64.5	66.1	68.3	70.9	73.9
0.23	56.1	58.9	59.5	64.6	65.3	66.8	69.3	72.5	74.5
0.33	58.2	60.9	61.6	64.5	66.2	67.1	70.0	72.3	74.3
0.43	59.2	63.5	63.5	66.9	68.2	68.6	70.4	72.5	74.0
0.55	59.8	64.7	65.5	67.4	68.8	69.7	70.7	72.8	74.8
0.65	62.0	65.1	66.7	69.0	69.4	71.2	72.4	73.3	75.3
0.89	66.2	67.7	68.8	70.2	70.9	72.3	73.4	74.0	75.9
1.04	66.7	70.5	70.6	71.3	73.2	73.4	74.1	75.0	76.3

Table 7 Statistical analysis of hardness as a function of cold work and nitrogen concentration

	Hardness = $\alpha + \beta[N]^{\gamma}$			Hardness = $a + k\,(CW, \%)^{n}$			
Cold work	α	β	γ	[N], wt%	a	k	n
0	50	16	0.74	0.06	51	4.7	0.37
10	63	8	1.1	0.43	59	3.2	0.36
30	68	6.5	1.0	0.65	62	3.0	0.35
50	67	6.7	1.1	1.04	66	2.7	0.29
Avg	63	7.9	1.12	Avg	60	2.9	0.38

received material, these values have a slight dependence on nitrogen concentration, increasing with increasing nitrogen concentration.

Regression analysis showed that the hardness increased with both cold working and nitrogen. However, examination of Fig. 14 and 15 showed there to be an interaction between nitrogen and cold working. Equation 10 is a linear combination of Eq 8 and 9 combined with a second-order term. An excellent statistical fit (R^2 = 0.99+) was obtained, requiring no additional term:

$$\text{Hardness (HRA)} = a + b[N,]^c + d[CW,]^e + f[N,\ wt\%]^c[CW\%]^e \qquad \text{(Eq 10)}$$

where a = 51.5, b = 15.7, c = 1.00, d = 4.24, e = 0.39, and f = −2.61. Correlation of Eq 10 to the previously derived tensile strain hardening (Eq 7) is more direct if percentage of cold work (Table 6) is changed to true strain:

$$\sigma_{true} = \ln\,(1 - \varepsilon\,[=1/\{1 - CW\} - 1]) \qquad \text{(Eq 11)}$$

The cold-working and strain-hardening coefficients determined from tensile and cold working were correlated (Table 8). The interaction terms were both negative and similar in magnitude. The nitrogen coefficients were also similar.

4. Discussion

The findings of this study, in which the nitrogen concentration in commercial-grade 201 SS was increased from 0.06 to 1.45 wt% by high-pressure melting, were consistent with previous findings for fcc steels with lower nitrogen concentration. Previous descriptions of the role of nitrogen-strengthening mechanisms centered on interstitial nitrogen. Results from this study showed that nitrogen strengthening continued even after nitrogen saturation had been reached and Cr_2N precipitates formed. Tensile tests and cold working showed that, provided that the nitride concentration was not too great (<2%) and the precipitates were evenly distributed throughout the matrix (i.e., not on grain boundaries), increasing the nitrogen concentration to levels greater than 1.0 wt% strengthened the steel in a very orderly manner.

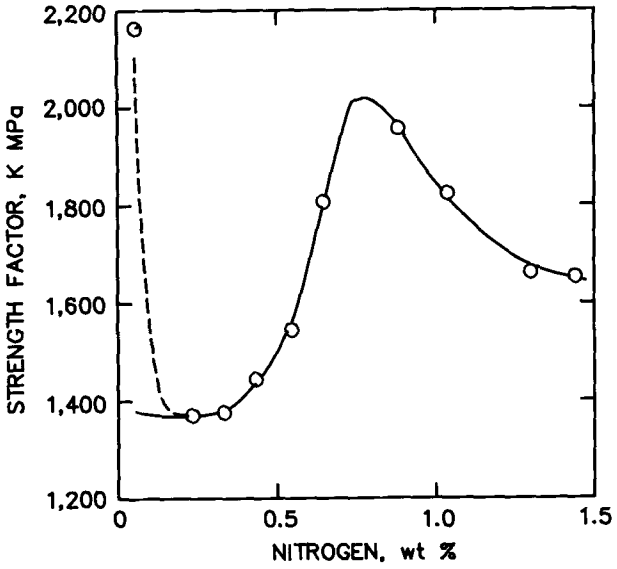

Fig. 13 Strength factor, K, as a function of nitrogen concentration. The strength factor of the as-received material is inconsistent with the high-pressure melted materials.

At room temperature, the yield-strengthening mechanism was approximately proportional to the square root of the nitrogen concentration, and the tensile-strengthening mechanism was between a linear nitrogen concentration and the square of the nitrogen concentration. A change in yield strength with the square root of the nitrogen concentration has been modeled by dislocation motion through a nonhomogeneous microstructure (Ref 31)—that is, a matrix with obstacles, where obstacles were randomly placed throughout the lattice (Ref 9, 20). In the present study, the obstacles were nitrogen-chromium clusters that resulted from the stronger bonding between nitrogen and chromium atoms rather than the weaker bonding between nitrogen and iron or nickel atoms. The stress necessary to generate dislocations and move them through the iron-chromium-nickel-nitrogen lattice (Peierls stress) was proportional to the matrix strength: As the interstitial nitrogen increased, the number of obstacles (i.e., the nitrogen-chromium cluster concentration) increased.

At low temperatures, the energy necessary for dislocation motion to move the dislocation through the matrix and around obstacles (i.e., dislocation climb) and the energy necessary for interstitial nitrogen to diffuse away from or to break free from the nitrogen-chromium cluster are both strong functions of temperature. Thus, the nitrogen concentration/mechanical strength relationships can be described as thermal, meaning that the yield-strengthening mechanism is a function of temperature.

At higher temperatures, the entire system has more energy, which allows for easier dislocation movement through the matrix. Thermal energy of the lattice and diffusion energy of the interstitial nitrogen are large enough that creep and diffusion no longer control dislocation movement. The plastic component

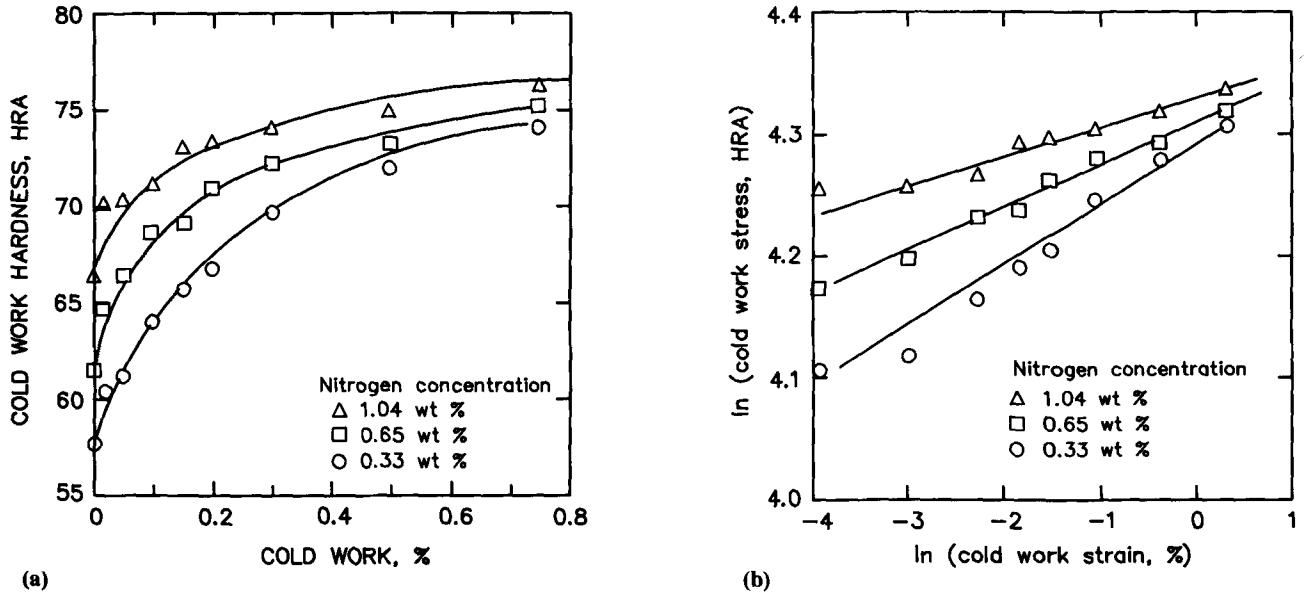

Fig. 14 (a) Hardness (HRA) as a function of cold working (%) for different nitrogen concentrations. (b) Log-log plot of hardness versus cold working for curves

of the true stress/true strain curve then becomes temperature independent.

Beyond the yield point, when dislocations were being generated and were moving throughout the lattice, changes in the stress-strain relationship developed. This happened because some of the interstitial nitrogen interacted with the dislocations and became attached to the dislocation line as the dislocations moved through the lattice. The movement of the dislocations was then impeded by the extra energy required to move both the dislocations and the attached nitrogen atoms. Thus, a synergistic interaction developed between the dislocation drag and the increase in dislocation concentration that resulted from the extended strain. The resulting relationship between nitrogen concentration and tensile strength is somewhere between linear and quadratic.

Previous TEM studies of dislocation motion in stainless steels and nitrogen-enhanced stainless steels (Ref 32-35) have shown that initial dislocation motion (for low strain levels) is dominated by dislocation cross-slip. The change in nitrogen concentration and distribution also changed the dislocation microstructure from a tangled dislocation microstructure at low strains and low nitrogen concentrations to a planar dislocation microstructure at increased strains and nitrogen concentrations. These changes in dislocation microstructure with increasing nitrogen concentration were reflected in the change in the strain-hardening exponent. At low strains and nitrogen concentration, the strain-hardening exponent was approximately 0.50, typical of tangled dislocation microstructures of fcc metal. At higher strains and nitrogen concentrations, the exponent rapidly decreased to approximately 0.20, typical of planar dislocation microstructures of bcc metals. The strain-hardening exponent is characteristic of dislocation generation and movement. For higher strain rates and nitrogen concentrations where the microstructure was planar, the strain-hardening exponent was constant and independent of nitrogen concentration.

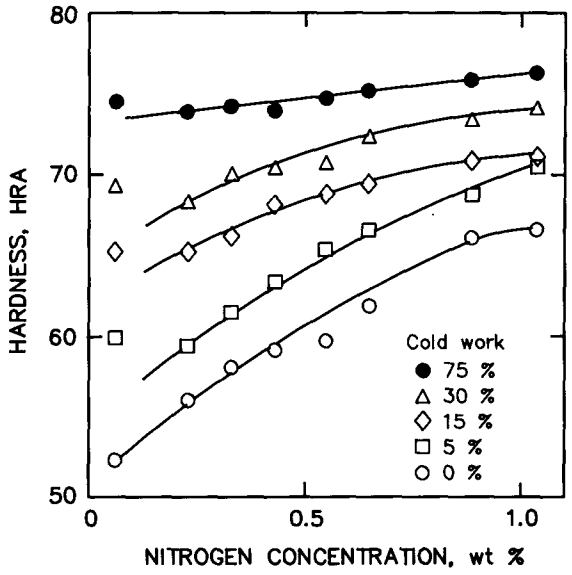

Fig. 15 Hardness (HRA) versus nitrogen concentration for several different cold-working conditions

Relationships between hardness and stress as a function of nitrogen concentration and either cold work or strain are summarized in Table 8. The change in elongation during cold working can be readily related to plastic strain deformation during tensile tests. Empirical correlations have been determined between hardness and tensile strength for steels (Ref 14). Thus, the strain-hardening exponent should be similar in hardness and stress. The cold-work data were obtained only after several percent cold-working reduction and thus should be related to the modified Ludwik equation presented in Table 4.

With increasing nitrogen concentrations, the change in tensile strength should also be similar to cold-working and tensile strengths. However, the measured effect of nitrogen on the different stresses—yield, breaking, and tensile—were quite different, varying from 0.72 for yield strength to 1.72 for breaking strength (Table 3). The statistically determined value of 1.37 in Table 8 is approximately that obtained for the tensile strength.

The nitrogen concentration/cold work interaction coefficients in stress and hardness equations used in Table 8 are negative. Thus, although both cold working and nitrogen can be used synergistically to improve tensile strength, at high stresses the role of nitrogen is reduced.

The greatest effect that nitrogen has on the strengthening of stainless steels is the increase in yield strength. Increasing the nitrogen concentration 1 wt% increased the yield strength by almost a factor of three, while the tensile strength increased only 50%.

5. Summary

Tensile and cold-work properties of nitrogen-enhanced commercial-grade 201SS were characterized. Nitrogen enhancement was obtained by high-pressure melting from 0.1 to 6.5 MPa, using nitrogen as the pressurizing gas. Nitrogen concentrations from 0.06 to 1.45 wt% were obtained. After melting, the nitrogen atoms were randomly dispersed throughout

Table 8 Hardness and stress correlation as a function of nitrogen, cold work, and strain

Coefficients	a	b	c	d	e	f
Hardness (HRA) = $a + b[N, wt\%]^c + {}^d(CW, \%)^e + f[N]^3(CW)^e$						
Cold work	51.7	15.7	1.00	4.24	0.39	–2.6
Hardness (HRA) = $a + b[N, wt\%]^c + d(\varepsilon)^e + f[N]^c(\varepsilon)^e$						
True strain	51.5	15.8	1.00	18.4	0.24	–12.9
Stress (MPa) = $a + b[N, wt\%]^c + d(\varepsilon)^e + f[N]^c(e)^e$						
	–93	595	1.36	487	0.23	–21.2
Modified Ludwik	...	568	1.37	1323	0.26	–13.3

the matrix. Nitrogen atoms were associated with solid-solution, randomly distributed chromium atoms.

Dislocation motion is controlled by dislocation interaction between nitrogen-chromium clusters and dislocation drag of nitrogen atoms associated with the dislocations. Nitrogen strengthening changes from a square root relationship of low strain rates to a linear/square relationship at higher strain rates. This results from a change in the deformation mechanism—from the dislocation motion being controlled by the interactions of dislocations with nitrogen-chromium clusters to a mechanism controlled by reduction in line tension due to segregation of nitrogen to the dislocations.

With increasing strain, dislocations begin to multiply and move through the lattice, and the nitrogen atoms now become associated with the dislocations. The higher-order dependence on nitrogen concentration resulted from (1) the interaction of the dislocations with the nitrogen-clusters, (2) the nitrogen drag component of the dislocations, and (3) the dislocation-dislocation interactions. The resulting dislocation microstructure is the planar array of dislocations that has been observed in stainless steels with higher nitrogen concentrations.

References

1. *Conf. Proc. HNS-88* (Lille, France), 18-20 May 1988, J. Foct and A. Hendry, Ed., Institute of Metals, London
2. *Conf. Proc. HNS-90* (Aachen, Germany), 10-12 Oct 1990, G. Stein and H. Witulski, Ed., Stahleisen, Dusseldorf
3. *Conf. Proc. HNS-93* (Kiev, Ukraine), 14-16 Sept 1993, V. Gavriljuk and V. Nadutov, Ed., Institute for Metal Physics
4. J. Rawers, G. Asai, R. Doan, and J. Dunning, *J. Mater. Res.*, Vol 7 (No. 5), 1992, p 1083-1092
5. J. Rawers, G. Asai, and R. Doan, *J. Mater. Sci.*, Vol 28 (No. 15), 1993, p 4028-4032
6. J. Rawers, G. Asai, and J. Dunning, *J. Mater. Res.*, Vol 9 (No. 12), 1994, p 3160-3169
7. F. Pickering, Some Beneficial Effects of Nitrogen Steel, *Conf. Proc. HNS-88* (Lille, France), 18-20 May 1988, J. Foct and A. Hendry, Ed., Institute of Metals, London, p 10-31
8. K. Jack, Nitrogen Precipitation—Retrospect and Prospect, *Conf. Proc. HNS-88* (Lille, France), 18-20 May 1988, J. Foct and A. Hendry, Ed., Institute of Metals, London, p 117
9. M. Grujicic, J.-O. Nilson, W.S. Owen, and T. Thorvaldson, Basic Deformation Mechanism in Nitrogen Strengthened Stable Austenitic Stainless Steels, *Conf. Proc. HNS-88* (Lille, France), 18-20 May 1988, J. Foct and A. Hendry, Ed., Institute of Metals, London, p 151-158
10. P.J. Uggowitzer and M. Harzenmouser, Strengthening of Austenitic Stainless Steels by Nitrogen, *Conf. Proc. HNS-88* (Lille, France), 18-20 May 1988, J. Foct and A. Hendry, Ed., Institute of Metals, London, p 174-179
11. M.O. Speidel, Properties and Applications of High Nitrogen Steels, *Conf. Proc. HNS-88* (Lille, France), 18-20 May 1988, J. Foct and A. Hendry, Ed., Institute of Metals, London, p 92-96
12. V.G. Gavriljuk and S. Jephimenko, Distribution of Nitrogen, *Conf. Proc. HNS-88* (Lille, France), 18-20 May 1988, J. Foct and A. Hendry, Ed., Institute of Metals, London, p 11-22
13. P.J. Uggowitzer and M.O. Speidel, Ultrahigh-Strength Austenitic Steels, *Conf. Proc. HNS-88* (Lille, France), 18-20 May 1988, J. Foct and A. Hendry, Ed., Institute of Metals, London, p 156-160
14. *Metals Handbook Desk Edition*, H. Boyer and T. Gall, Ed., American Society for Metals, 1985, chap. 15
15. J. Rawers, N. Gokcen, and R. Pehlke, *Metall. Trans. A*, Vol 24A, 1993, p 73-85
16. H. Wriedt, N. Gokcen, and R. Hafziger, *Bull. Alloy Phase Diag.*, Vol 8 (No. 4), 1987, p 355-377
17. G. Stein, J. Menzel, and H. Dorr, Industrial Manufacture of Massive Nitrogen Alloyed Steels, *Conf. Proc. HNS-88* (Lille, France), 18-20 May 1988, J. Foct and A. Hendry, Ed., Institute of Metals, London, p 32-39
18. J. Rawers and L.J. Rawers, *J. Mater Sci. Lett.*, Vol 10, 1991, p 1101-1109
19. M. Kikuchi, M. Kajihara, and K. Frisk, Solubility of Nitrogen in Austenitic Stainless Steels, *Conf. Proc. HNS-88* (Lille, France), 18-20 May 1988, J. Foct and A. Hendry, Ed., Institute of Metals, London, p 63-74
20. M. Byrnes, M. Grujicic, and W. Owen, *Acta Metall.*, Vol 35 (No. 7), 1987, p 1853-1862
21. R. Reed and N. Simon, Nitrogen Strengthening of Austenitic Stainless Steels at Low Temperature, *Conf. Proc. HNS-88* (Lille, France), 18-20 May 1988, J. Foct and A. Hendry, Ed., Institute of Metals, London, p 180-188
22. J. Low and F. Garofalo, *Proc. Soc. Stress Anal.*, Vol 4, 1947, p 16-32
23. H.J. Kleemola and M. Nieminen, *Metall. Trans.*, Vol 5, 1974, p 1863-1866
24. D.C. Ludwigson, *Metall. Trans.*, Vol 2, 1971, p 2825-2828
25. A. Soussan, S. Degallaix, and T. Magnin, *Mater. Sci. Eng.*, Vol 142A, 1991, p 169-176
26. P. Ludwik, *Elemente der Technologischen Mechanik*, Springer, Berlin, 1909, p 32 (in German)
27. J. Hollomon, *Trans. AIME*, Vol 162, 1945, p 268-273
28. J. Simmons, Influence of Nitride Precipitation on the Plastic Flow Behavior of High-Nitrogen Austenitic Stainless Steel, *Acta Metall.*, Sept 1994, accepted for publication
29. G.J. Slavens and J.S. Dunning, High-Pressure Furnace for Alloying Steels with Nitrogen, *High Temp.—High Press.*, Vol 26, 1994, p 134-147
30. H. Swift, *J. Mech. Phys. Solid*, Vol 1, 1952, p 1-18
31. J. Friedel, *Dislocations*, Addison-Wesley, London, 1967
32. S.W. Yang and J.E. Spruiell, *J. Mater. Sci.*, Vol 17, 1982, p 677-690
33. H. Chandra Holm, P. Uggowitzer, and M. Speidel, *Scr. Metall.*, Vol 21, 1987, p 513-518
34. J. Sassen, A. Garratt-Reed, and W.S. Owen, Electron Microscopy of Austenitic Fe-Ni-Cr Alloys Containing Nitrogen, *Conf. Proc. HNS-88* (Lille, France), 18-20 May 1988, J. Foct and A. Hendry, Ed., Institute of Metals, London, p 159-162
35. G. Wahlberg, U. Rolander, and H.-O. Andren, Interaction between Nitrogen and Substitutional Elements in the Austenitic Phase of Duplex Austenitic Ferritic Stainless Steels, *Conf. Proc. HNS-88* (Lille, France), 18-20 May 1988, J. Foct and A. Hendry, Ed., Institute of Metals, London, p 163-168